

## NUMERICAL SIMULATIONS OF GLOBULAR CLUSTER FORMATION

NAOHITO NAKASATO<sup>1</sup>, MASAO MORI<sup>2</sup>, AND KEN'ICHI NOMOTO<sup>1,3</sup>

*To appear in the Astrophysical Journal 2000*

### ABSTRACT

We examine various physical processes associated with the formation of globular clusters by using the three-dimensional Smoothed Particle Hydrodynamics (SPH) code. Our code includes radiative cooling of gases, star formation, energy feedback from stars including stellar winds and supernovae, and chemical enrichment by stars. We assume that, in the collapsing galaxy, isothermal cold clouds form through thermal condensations and become proto-globular clouds. We calculate the size of proto-globular clouds by solving the linearized equations for perturbation. We compute the evolution of the inner region of the proto-cloud with our SPH code for various initial radius and initial composition of gases. When the initial gases contain no heavy elements, the evolution of proto-clouds sensitively depends on the initial radius. For a smaller initial radius, the initial star burst is so intense that the subsequent star formation occurs in the central regions to form a dense star cluster as massive as the globular cluster. When the initial gases contain some heavy elements, the metallicity of gases affects the evolution and the final stellar mass. If the initial radius of the proto-globular clouds was relatively large, the formation of a star cluster as massive as the globular clusters requires the initial metallicity as high as  $[\text{Fe}/\text{H}] \geq -2$ . The self-enrichment of heavy elements in the star cluster does not occur in all cases.

*Subject headings:* globular clusters: general — galaxies:star clusters — stars: formation — hydrodynamics

### 1. INTRODUCTION

The globular clusters belong to the oldest populations in our galaxy. For the general reviews on globular clusters, see Meylan, & Heggie (1997) and Harris (1991). Their formation (Elmergreen et al. 1999) is closely related to the formation process of our galaxy. The formation of a globular cluster may take place in two stages: (1) the formation of a proto-globular cloud (PGC) and (2) the formation of a star cluster from the PGC. There are three scenarios for the formation of a PGC, denoted as primary, secondary, and tertiary model (Fall & Rees 1987), where the PGC forms in different stages, i.e., before, during, or after the collapse of the galaxy, respectively.

- The primary model was suggested by Peebles & Dicke (1968). They showed that the Jeans mass of the recombination stage of the universe is comparable to the observed masses of globular clusters and thus the PGC can form due to the gravitational instability. Globular clusters may be debris of these objects. The most serious problem with this primary model is that there have been few intergalactic globular clusters discovered. Almost all globular clusters ever discovered exist in galaxies.
- In the secondary model, on which we concentrate in the present paper, the PGC forms due to thermal instabilities (Fall & Rees 1985). Our detailed investigation and calculation are presented in the following sections.
- For the tertiary model, one example is that globu-

lar clusters form from large-scale unorganized motion of interstellar gas as in the Magellanic Clouds, which are now producing young clusters (Kumai, Basu, & Fujimoto 1993). Another example is that very young globular clusters are observed in nearby galaxy NGC 1705 and 1569 (Ho & Filippenko 1996).

Once the PGC forms, there might be many ways to form a globular cluster (GC). Murray & Lin (1993) summarized the scenarios of the formation of GCs from PGCs as follows. The PGC can be divided into two types depending on their masses. The cloud, whose mass exceeds the Jeans mass, is gravitationally unstable, thus spontaneously collapsing to form stars. The cloud, whose mass is smaller than the Jeans mass, is stable until some instabilities are introduced. A cloud-cloud collision or cloud-disk collision can trigger such instability. When such collisions occur, the cloud would become thermally unstable owing to the efficient cooling. This cooling would lead to the formation of a very dense region, thus inducing a burst of star formation.

In the present paper, we examine quantitatively the above still qualitative scenario of the globular cluster formation. We use our Smoothed Particle Hydrodynamics (SPH) code (Lucy 1977; Gingold & Monaghan 1977) to simulate the formation of a globular cluster from a PGC. Our code includes the following physical processes: radiative cooling, star formation, energy feedback from stars including stellar winds and supernovae, and chemical enrichment from stars. The SPH method which includes star formation processes like ours has been applied to many astrophysical problems. Such problems include the formation of

<sup>1</sup>Department of Astronomy, School of Science, University of Tokyo, Bunkyo-ku, Tokyo 113-0033; nakasato@astron.s.u-tokyo.ac.jp, nomoto@astron.s.u-tokyo.ac.jp

<sup>2</sup>Institute of Astronomy, School of Science, University of Tokyo, Mitaka, Tokyo 181-8588; mmori@mtk.ios.s.u-tokyo.ac.jp

<sup>3</sup>Research Center for the Early Universe, School of Science, University of Tokyo, Bunkyo-ku, Tokyo 113-0033

isolated galaxies (Katz 1992; Steinmetz & Müller 1994), the evolution of galaxies (Friedli & Benz 1995), and the cosmological simulations (Navarro & White 1993). However, our study is the first attempt to apply this method to the globular cluster formation (preliminary results have been presented in Nakasato et al. (1996); Nakasato, Mori, & Nomoto (1999)).

Among the two triggers of the instability, collapse and collision, we concentrate on the collapse case in the present paper. The collision case for a wide range of parameters (masses of the two clouds, a relative velocity between the clouds etc.) will be discussed elsewhere. This paper consists of the following sections. In section 2 our SPH method is described. In section 3, we present our linear analysis for the thermal instabilities to form a PGC. In section 4, we present the results of the evolution of the PGC with two different initial compositions of gases. Sections 5 and 6 are devoted to discussions and concluding remarks, respectively.

## 2. METHOD

To simulate the formation of a star cluster from gases, we use our GRAPE-SPH code using Remote-GRAPE library (Nakasato, Mori, & Nomoto 1997). The GRAPE is a special purpose computer for the self gravity calculations in general N-body system (Sugimoto et al. 1990). Our GRAPE-SPH code includes various physical processes, e.g., radiative cooling, star formation, and feedback from formed stars. There are many different implementations of the SPH method (a recent comparison of various SPH implementations is presented in Thacker et al. (1998)). In the present paper, we describe an essential point of our SPH code. The SPH formulation that we use is the same as the described in Navarro & White (1993). We use the smoothing length that can vary spatially and evolve with time, and integrate equations of motion with a second order Runge-Kutta method as described in Navarro & White (1993). Details of the implementation of our code are described in Mori et al. (2000). In the following subsections, we describe the physical processes (cooling, star formation, and feedback) in some detail.

### 2.1. Radiative cooling

The radiative cooling rates depend on the temperature and ionization states of the gas. Also, the chemical composition of the gas affects the cooling rate drastically. We perform SPH simulations for the following three cases (A, B, C) of the gas with different physical state and chemical composition.

Case A: We assume that the chemical composition of the gas is primordial with no heavy elements and the gas is in ionization equilibrium. In this case, our treatment of radiative cooling is essentially the same as adopted by Katz, Weinberg, & Hernquist (1995); they computed the cooling rate using the two-body processes of H and He, and free-free emissions. The cooling function ( $\Lambda(T)$ ) is shown in Figure 1 with the solid line. In this case, the cooling rate decreases very rapidly as the temperature  $T$  decreases below  $2 \times 10^4$  K so that the gas would not radiatively cool below  $T \sim 10^4$  K.

Case B: We assume that the gas includes some heavy elements and is in ionization equilibrium. In this case, we use the cooling function with different chemical com-

position that is computed by MAPPINGS III software by R.S. Sutherland (MAPPINGS III is the successor of MAPPINGS II that is described in Sutherland & Dopita (1993)). We compute the cooling function of the ionization equilibrium gas for  $[\text{Fe}/\text{H}] = -5.0 - 0.0$  with the solar abundance ratio (see Table 4 of Sutherland & Dopita (1993)) and present the results in Figure 1 with the dashed lines (each line corresponds to  $[\text{Fe}/\text{H}] = -1, -2, -3$  respectively from the top to the bottom). Existence of heavy elements significantly enhances the cooling rates. At  $T < 10^4$  K, the cooling due to the forbidden line emission of carbon and oxygen is efficient. For  $[\text{Fe}/\text{H}] = -1$ , the cooling rates around  $T \sim 10^5$  K are 100 times larger than the cooling rates of primordial hydrogen and helium gas. These differences would make the evolution of the gas very different.

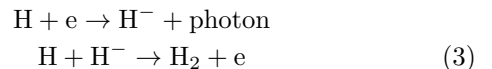
Case C: We concern about the non-equilibrium cooling. If the gas cools from high temperatures, ionization equilibrium is not realized. Figure 2 shows the ratio between the recombination time ( $t_{\text{recom}}$ ) of hydrogen and the cooling time ( $t_{\text{cool}}$ ) of primordial gas in ionization equilibrium;  $t_{\text{recom}}/t_{\text{cool}}$ . The  $t_{\text{recom}}$  and  $t_{\text{cool}}$  are defined as

$$t_{\text{recom}} = \frac{1.0}{\alpha(T)f_e(T)} \quad (1)$$

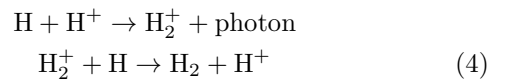
and

$$t_{\text{cool}} = \frac{3k_b T}{2\Lambda(T)}, \quad (2)$$

where the  $\alpha$  is the recombination coefficient of hydrogen and electron,  $f_e$  is the fraction of free electrons, and  $k_b$  is the Boltzman constant. For  $\alpha$ , we use the value of Spitzer (1978). Clearly, the cooling time is much shorter than the recombination time for  $T \sim 2 \times 10^4$  K, so that ionization equilibrium is not realized when the gas cools from high temperatures. In the non-equilibrium case, the existence of electrons and ionized hydrogen at  $T < 10^4$  K makes it possible to form  $\text{H}_2$  molecules through the creation of intermediaries  $\text{H}^-$  and  $\text{H}_2^+$  as:



and



(Shapiro & Kang 1987). These  $\text{H}_2$  molecules cause further cooling down to  $T \sim 10^2$  K owing to the rotational-vibrational line excitation.

To include the effect of such molecular cooling, we have to solve rate equations that determine the ionization states of H and He atoms, and the formation and destruction of  $\text{H}_2$  molecules. In our case, the typical time step in solving the rate equations is shorter than the dynamical time step, which is determined mainly by the Courant condition. Integrating all equations with a shorter timestep than the dynamical time is very costed work. So we divide the dynamical timestep with dynamical variables (density etc.) being constant in solving the energy and rate equations, which is similar to the method adopted in Shapiro & Kang

(1987). The rate-coefficients are also the same as used in Shapiro & Kang (1987). Included species are  $\text{H}^0$ ,  $\text{H}^+$ ,  $\text{He}^0$ ,  $\text{He}^+$ ,  $\text{He}^{++}$ ,  $\text{H}^-$ ,  $\text{H}_2^+$ ,  $\text{H}_2$ ,  $\text{H}_2^*$  and  $e$ , where  $\text{H}_2^*$  is the excited hydrogen molecule. In our SPH code, we solve the rate equations for 10 species in each SPH particle with a reasonable computing time. Solving the rate equations for the gas including heavy elements (over 200 species) is not feasible with a current resource so that we only concern the hydrogen and helium plasma in the present paper.

The cooling function for the non-equilibrium case is presented in Figure 1 with the dotted line. In computing these cooling rates, we follow the isobaric temperature evolution of the fully ionized gas. Initially, the temperature and hydrogen number density of the gas are  $10^7$  K and  $0.01 \text{ cm}^{-3}$ , respectively. We assume optically thin plasmas so that the gas cools rapidly. Around  $T \sim 2 \times 10^4$  K,  $\text{H}_2$  molecules begin to form. At  $T < 10^4$  K, the cooling rate due to  $\text{H}_2$  molecules is comparable to the cooling rate for  $[\text{Fe}/\text{H}] = -1$  gas.

Finally, we summarize the treatment of the cooling rates in our SPH code. We can perform SPH simulations for these three cases A, B and C. In the present paper, we will study the evolution of a PGC with two different initial chemical compositions, e.g., a metal-free gas cloud and a metal-rich gas cloud. In the former case, we solve the energy and rate equations simultaneously for each SPH particle (case B) if the gas temperature is lower than  $3 \times 10^4$  K and the gas particle is not in the heating phase (see section 2.3). If these conditions are met, we use the pre-computed cooling table for the ionization equilibrium case (case A). In the latter case, we use the pre-computed cooling table to solve the energy equations (case C).

## 2.2. Star formation

Our treatment of star formation is the same as adopted by Katz (1992). Hereafter, ‘‘STAR’’ means ‘‘star particle’’, which is not an individual star but an association of many stars. A STAR forms in the region where the flow is converging, cooling, and Jeans unstable. These conditions are expressed as

$$(\nabla \cdot \mathbf{v})_i < 0, \quad (5)$$

$$t_{\text{cool}} < t_{\text{d}}, \quad (6)$$

$$t_{\text{d}} < t_{\text{sound}}. \quad (7)$$

Here  $t_{\text{cool}}$ ,  $t_{\text{d}}$ , and  $t_{\text{sound}}$  are the cooling time, dynamical time, and sound crossing time, respectively, and expressed as

$$t_{\text{cool}} = \frac{\mu^2 u}{\rho \Lambda}, \quad (8)$$

$$t_{\text{d}} = \frac{1}{\sqrt{4\pi G \rho}}, \quad (9)$$

$$t_{\text{sound}} = \frac{h_i}{c_s}, \quad (10)$$

where  $\mu$  is the mean molecular weight,  $u$  is the specific thermal energy, and  $c_s$  is the local sound speed. A STAR forms in the region where these all three conditions are satisfied. The star formation rate is given as

$$\frac{D\rho_*}{Dt} = -\frac{\rho}{t_{\text{starform}}} = -C\sqrt{4\pi G}\rho^{\frac{3}{2}}, \quad (11)$$

where  $\rho_*$  is the density of a star, and  $t_{\text{starform}} = t_{\text{d}}/C$  with a star formation parameter  $C$ . In the present paper, we adopt  $C = 1.0$ , i.e., a STAR forms in a dynamical time. The last term of equation 11 is similar to the Schmidt’s law (Schmidt 1959). Integrating equation (11) over one time step  $\delta t$  and making calculations with the equations for SPH, we obtain the mass of a newly formed star in  $\delta t$  as

$$m_{\text{star}} = \left[ 1 - \frac{1}{1 + 0.5 \frac{\delta t}{t_{\text{starform}}}} \right] \pi h_i^3 \rho_i. \quad (12)$$

The newly formed STAR is then treated as a collision-less particle. We introduce the minimum allowed mass ( $\sim 10 M_{\odot}$ ) for the newly formed STAR to prevent the unphysical effects in the equation of motion and the treatment of the feedback processes.

We note the star formation recipes in our SPH code. In the regions with increasing densities, first two conditions for the star formation (Eq. 5 and 6) are almost satisfied. Thus whether STAR forms in some regions is determined mostly by the Jeans criterion (Eq. 7). The critical density for the star formation in our treatment is obtained as

$$\rho_{\text{Jeans}} > \left( \frac{\gamma b}{4\pi G \mu m} \right)^3 \frac{1}{m_i^2} T^3 \left( \frac{1}{\beta^6} \right). \quad (13)$$

Here, it is assumed that the neighbor radius is expressed as

$$h_i = \beta \left( \frac{m_i}{\rho_i} \right)^{1/3}, \quad (14)$$

where  $\beta$  is determined experimentally, because  $h_i$  is determined in order to make the number of neighbor particles almost constant in some range (30 - 80 in our codes). Since the typical value of  $\beta$  is 1.0 - 1.1,  $\beta^6$  ranges 1.0 - 2.0. Then if  $m_i$  is constant, the critical density is determined almost only by the temperature. The typical calculations in the present paper use 5000 gas particles for a  $10^6 M_{\odot}$  gas sphere. Thus the initial mass per particle ( $m_i$  in Eq. 13) is  $\sim 200 M_{\odot}$ . For  $T = 10^4$  K and  $10^2$  K, the critical density for star formation is  $\rho_{\text{Jeans}} \sim 10^{-17}$  and  $10^{-23} \text{ g cm}^{-3}$ , respectively. With the star formation recipes used in our SPH code, the STAR forms only in the very high density region if  $T \sim 10^4$  K. There are, however, the maximum density ( $\rho_{\text{max}}$ ) that numerically reached in the SPH method; it is estimated

$$\rho_{\text{max}} \sim \frac{N_n m_i}{\epsilon^3}, \quad (15)$$

where  $N_n$  is the number of neighbor particles and  $\epsilon$  is the gravitational softening length. In the present calculations,  $\rho_{\text{max}} \sim 1.8 \times 10^{-20} \text{ g cm}^{-3}$ . These arguments ensure that with the star formation recipes used in our SPH code and the initial conditions of the present calculations, the STAR forms in the region where the temperature is as low as  $10^2$  K.

### 2.3. Feedback

The formed stars eject gases and heavy elements in stellar winds and Type II supernova explosions and heats up, accelerate, and enrich a circumstellar and an interstellar medium. High energy explosions like supernova produce high temperature and low density regions in interstellar medium. In the SPH method, the numerical accuracy for high density regions is much better than mesh based methods but the accuracy for low density regions are poorer. A typical resolution of usual SPH simulations, e.g., Navarro & White (1993), including a star formation process (100 - 1000 pc) is larger than a typical size of supernova remnants (< 100 pc). Thus, it is difficult to properly include the energy, momentum, and mass release from stars in the SPH method because of the nature of the SPH method and the poor resolutions in current computing resources. We must use some approximations to mimic real feedback processes in the SPH method.

One of the method has been proposed by Navarro & White (1993). In their method, the energy produced by a supernova explosion is distributed to neighbor gas particles of each STAR mostly as a thermal energy and the rest is distributed as a velocity perturbation to the gas particles; the fraction of the energy in a kinetic form is a free parameter (we note that Leitherer, Robert, & Drissen (1992) presented the population synthesis model of stellar feedback processes). In the present paper, we distribute the energy to neighbor particles in a pure thermal form as a zero-th order approximation, because the size and time scale of our model are much smaller than those of a galaxy formation model of Navarro & White (1993).

#### 2.3.1. Energy ejection

The energy ejection rate per STAR is given as

$$E_{\text{eject}} = e_{\text{SW}}R_{\text{SW}} + e_{\text{SNII}}R_{\text{SNII}}, \quad (16)$$

where  $e_{\text{SW}}$  is the total energy ejected by stellar winds during the stellar lifetime and  $e_{\text{SNII}}$  are the energy ejected by one Type II supernova explosion. The  $R_{\text{SW}}$  is the number of stars per unit time expelling their envelopes at the current epoch and  $R_{\text{SNII}}$  is the rate of Type II supernovae. We define the  $R_{\text{SW}}$  and  $R_{\text{SNII}}$  as follows

$$R_{\text{SW}} = \frac{\int_{M_{\text{ms}}}^{M_{\text{up}}} \Phi(m)dm}{\tau(M_{\text{ms}})} \quad (17)$$

$$R_{\text{SNII}} = \frac{\int_{M_{\text{ms}}}^{M_{\text{ma}}} \Phi(m)dm}{\tau(M_{\text{ms}}) - \tau(M_{\text{ma}})}, \quad (18)$$

where  $\Phi(m)$  is the initial mass function (IMF), namely  $\Phi(m)dm$  gives the number of stars in the mass range of  $(m, m + dm)$  and the  $\tau(m)$  is the stellar lifetime (David, Forman, & Jones 1990). In the present study, we assume the power law type IMF as

$$\Phi(m) = Am^{-2.35}, \quad (19)$$

where the  $A$  is the constant. For the upper and lower limit masses in Eq. (19),  $M_{\text{up}} = 120 M_{\odot}$  and  $M_{\text{lo}} = 0.05$

$M_{\odot}$  are assumed. In Eq. (17) and (18),  $M_{\text{ma}} (= 50.0 M_{\odot})$  and  $M_{\text{ms}} (= 8.0 M_{\odot})$  are the upper and lower limit masses of the stars that explode as Type II supernovae.

For the supernova energy, we assume that  $e_{\text{SNII}} = 10^{51}$  erg. For the stellar wind,  $e_{\text{SW}}$  is estimated to be  $0.2 \times 10^{51}$  erg for solar metallicity stars from the observational data of OB associations (Abbot 1982). The Chemical abundance of a massive star significantly affects  $e_{\text{SW}}$  (Leitherer, Robert, & Drissen 1992), so that we use metallicity dependent  $e_{\text{SW}}$  as  $e_{\text{SW}} = 0.2e_{\text{SNII}}(Z/Z_{\odot})^{0.8}$ , where  $Z$  is the mass fraction of metal in the STAR.

#### 2.3.2. Mass ejection

In our code, the mass ejection due to stellar winds is combined with the mass ejection due to Type II supernova. Thus, the mass ejection rate per STAR is written as

$$M_{\text{eject}} = m_{\text{SNII}}R_{\text{SNII}}, \quad (20)$$

where  $m_{\text{SNII}}$  is the average mass ejected by stellar winds and Type II supernovae defined as

$$m_{\text{SNII}} = \frac{\int_{M_{\text{ms}}}^{M_{\text{ma}}} m\Phi(m)dm}{\int_{M_{\text{ms}}}^{M_{\text{ma}}} \Phi(m)dm} - m_{\text{NS}}, \quad (21)$$

Here  $m_{\text{NS}}$  is the mass that is locked up in the neutron star and assumed to be  $1.4 M_{\odot}$ . The fraction of heavy metal in  $M_{\text{eject}}$  is computed by the nucleosynthesis yield of Type II supernovae (Tsujimoto et al. 1996; Nomoto et al. 1997).

#### 2.3.3. Summary

We assume that the feedback phase continues for  $\tau(M_{\text{ms}}) = 4.3 \times 10^7$  yr from the formation of each STAR and is divided into two phases: a stellar wind phase and a supernova phase. The stellar wind phase continues for  $\tau(M_{\text{ma}}) = 5.4 \times 10^6$  yr, during which only the energy ejection from STARS is included; the ejected mass is included in the supernova phase for simplicity. The supernova phase begins at  $t = \tau(M_{\text{ma}})$  and ends at  $t = \tau(M_{\text{ms}})$ . During the supernova phase, the energy ejection is given by Eq. (16). The mass ejection is the sum of the contributions by the stellar winds and Type II supernovae.

The thermal energies, gases, and heavy elements from stellar winds and supernovae are smoothed over neighbor particles of the STAR within a neighbor radius of  $R_f$  (feedback radius). We treat  $R_f$  as a parameter to meet the observational constraints. Such neighbor particles are called ‘‘in heating phase’’. When the gas particles are in heating phase, we assume that the cooling is suppressed as proposed in Mori, Yoshii, & Nomoto (1999). This treatment produces the high temperature region around the STAR. Thus, the star formation is forbidden in the gas particles in heating phase.

## 3. PROTO-GLOBULAR CLOUD FORMATION

We first examine the radiative condensations, which occur in a wide range of astrophysical circumstances from solar prominence to interstellar clouds (Meerson 1996). Radiative condensations in optically thin plasma have been considered by many authors since the pioneering work by

Parker (1953) and Field (1965). The scale length of gravitational instability in a collapsing proto-galaxy is much larger than the radii of globular clusters (Lin & Murray 1996). As will be shown in the following sections, the scale length of radiative condensations is comparable to the radii of globular clusters. Thus, in a collapsing proto-galaxy, radiative condensations may be the only mechanism to form a PGC (Fall & Rees 1985; Lin & Murray 1996).

### 3.1. Radiative condensations in a collapsing proto-galaxy

The characteristic equation for the growth rate of radiative condensations,  $n$ , is obtained from the linearized equations for perturbations as

$$n^3 + n^2 c_s \left( k_T + \frac{k^2}{k_K} \right) + n c_s^2 k^2 + \frac{c_s^3 k^2}{\gamma} \left( k_T - k_\rho + \frac{k^2}{k_K} \right) = 0, \quad (22)$$

where  $c_s$  is the sound speed,  $\gamma$  is the ratio of the specific heats,  $k = 2\pi/\lambda$  is the wavenumber of the perturbation,  $k_\rho$  and  $k_T$  are the wavenumber of sound waves whose frequencies are equal to the growth rate of isothermal and isochoric perturbation, respectively, and  $k_K$  is the inverse of the scale length of thermal conduction (Field 1965).  $k_\rho$ ,  $k_T$  and  $k_K$  are expressed as

$$k_\rho = \frac{\mu(\gamma - 1)\rho_0}{ck_b T_0} \frac{\Lambda(T_0)}{\mu^2}, \quad (23)$$

$$k_T = \frac{\mu(\gamma - 1)\rho_0}{ck_b} \frac{d\Lambda}{\mu^2 dT}, \quad (24)$$

$$k_K = \frac{ck_b \rho_0}{\mu(\gamma - 1)\kappa}, \quad (25)$$

where  $T_0$  and  $\rho_0$  are the equilibrium temperature and density, respectively,  $k_b$  is the Boltzmann constant, and  $\Lambda(T)$  is the cooling function (Figure 1). We assume  $\gamma = 5/3$  and  $\kappa = 5.6 \times 10^{-7} T^{2.5} \text{ erg s}^{-1} \text{ K}^{-1} \text{ cm}^{-1}$ . Solving Eq. (22) as a cubic equation of  $n$  for different  $k$ , we obtain the dispersion relation between  $n$  and  $k$ . In applying to our galaxy, we adopt  $T_0 \sim 1.0 \times 10^6 \text{ K}$  and  $\rho_0 \sim 1.7 \times 10^{-24} \text{ g cm}^{-3}$  (Fall & Rees 1985). With these values, the dispersion relation has a peak at some  $k$ . In the present paper, we assume that the scale for the maximum growth rate is typical scale of a PGC. To obtain the typical scale of a PGC for different  $T_0$  and  $\rho_0$ , equation (22) is viewed as a quadratic in  $k^2$  (see Section II (d) in Field (1965)).

The results for different  $T_0$  and  $\rho_0$  are presented in Figure 3. In applying to our galaxy, we obtain the scale length of  $\sim 600 \text{ pc}$ . This scale length is consistent with the following simple estimate. For the adopted cooling function, the wavelengths for  $k_\rho$  and  $k_K$  with  $T_0 \sim 1.0 \times 10^6 \text{ K}$  and  $\rho_0 \sim 1.7 \times 10^{-24} \text{ g cm}^{-3}$  are respectively obtained as

$$\lambda_\rho > 10^3 \text{ pc} \quad \text{and} \quad \lambda_K < 1 \text{ pc}. \quad (26)$$

This implies that the perturbation with a scale greater than  $10^3 \text{ pc}$  is dumped owing to the limit of the sound speed, and the perturbation with a scale smaller than  $1 \text{ pc}$  is also dumped by thermal conduction. Thus the typical scale of a PGC in our galaxy is estimated to be several hundreds pc and the mass of a PGC ranges from  $10^7$  to  $10^8 M_\odot$ .

### 3.2. Density profile of a PGC

The estimated scale of a PGC is larger than the present radius of globular clusters (10 - 100 pc). This implies that during radiative condensations, a PGC shrinks before star formation begins or star formation in a PGC occurs in the central region of the cloud. If we consider the metal-free PGC where the ionization equilibrium is achieved, the cooling time,  $t_c$ , of the PGC is much shorter than the dynamical time,  $t_d$  ( $t_c/t_d \sim 0.25$  for  $T_0 \sim 1.0 \times 10^6 \text{ K}$  and  $\rho_0 \sim 1.7 \times 10^{-24} \text{ g cm}^{-3}$ ). After the short period of radiative condensations ( $\sim t_c$ ), the PGC becomes a warm dense cloud ( $T \sim 10^4 \text{ K}$ ) surrounded by a hot thin gas with  $T_0$  (Fall & Rees 1985).

The qualitative discussion on the evolution of such a metal-free PGC has been presented by Lin & Murray (1996). They argued that in the first stage of collapsing galaxy, the assumption of ionization equilibrium is not valid because of little radiative emission. If the ionization equilibrium is not achieved, the temperature of high density regions can be as low as  $\sim 10^2 \text{ K}$  due to hydrogen molecular cooling. In this case, the high density cold cloud with  $T = 10^2 \text{ K}$  is surrounded by a warm gas. The critical mass of the isothermal sphere confined by an external pressure depends on the cloud temperature (Ebert 1955; McCrea 1957). If the temperature of the cloud is  $\sim 10^2 \text{ K}$ , the critical mass is  $\sim 10^2 M_\odot$ . According to Lin & Murray (1996), such a small cloud as  $M \sim 10^2 M_\odot$  collapses to make the first stars in the proto-galaxy. These first generation stars are the source of radiative emission to maintain the ionization equilibrium. If such radiation continues long enough, a cold PGC will evolve almost isothermally with  $T \sim 10^4 \text{ K}$  and form the isothermal profile of  $\rho \propto r^{-2}$ . The core size of the PGC will decrease from the initial size of several hundreds pc to a size comparable to the observed globular cluster. According to these arguments, we can assume that the density structure of a PGC has a form of  $\rho \propto r^{-2}$ .

For the initial conditions of the PGC, we use the King profile with fixed mass of  $M \sim 10^6 M_\odot$  which nearly equals to the Jeans mass of the current conditions ( $\rho_0$  and  $T_0$ ). We assume that this sphere represents the inner regions of the PGC. We examine three different cases for a initial radius of  $R_i = 150, 200, \text{ and } 300 \text{ pc}$ . The initial gas density profiles of the three cases are presented in Figure 4. For the smaller  $R_i$ , the initial concentration of the inner region of the PGC is higher. The temperature of the sphere is assumed to be  $T \sim 10^4 \text{ K}$ . The properties of the inner region of the PGC, which are the initial conditions of our calculations, are summarized as follows:

- The mass of the clouds is  $M \sim 10^6 M_\odot$ .
- The radius of the clouds is  $R_i \sim 150 - 300 \text{ pc}$ .
- The clouds is an isothermal sphere with  $T \sim 10^4 \text{ K}$ .
- Initially, the velocity of the cloud is zero.

In the following calculations, the initial number of gas particles is  $\sim 5000$  so that the initial mass of the one gas particle is  $\sim 200 M_\odot$ . The dependence of varying the initial number of gas particles is discussed in Section 4.3. In all cases, the gravitational softening length for all particles is set to be  $1 \text{ pc}$  and fixed during the calculations.

## 4. RESULTS

First, we note on the feedback radius ( $R_f$ ). We use the Strömgen radius ( $R_{St}$ ) of a typical OB star as  $R_f$ . The typical value is  $R_{St} \sim 10 - 100$  pc, where the density of the ISM is  $\sim 1 \text{ cm}^{-3}$  (Osterbrock 1974). The radius depends on the density of the ISM as  $R_{St} \propto n^{-2/3}$ . In the central region of our initial models,  $n$  ranges from  $100 \text{ cm}^{-3}$  to  $1000 \text{ cm}^{-3}$ . Thus, we can estimate  $R_f \sim 1 - 5$  pc (using the largest value of  $R_{St}$ ). In the following two subsections, we choose  $R_f = 3$  pc for all gas particles. The results for both cases are summarized in Table 1. The results for different  $R_f$  are described in Section 4.3.

## 4.1. Evolution of the metal-free PGC

In this section, we describe the evolution of the metal-free PGC for case C.

As presented in the previous sections, the metal-free PGC may evolve isothermally with  $T \sim 10^4$  K. The isothermal evolution of PGC is terminated when the ionizing radiations from the first generation stars stop. Without ionizing radiation, the PGC cools efficiently by  $\text{H}_2$  molecules. Our calculations start from that time when the PGC begins to cool. We assume  $M = 10^6 M_\odot$ , and the initial temperature of  $T = 10^4$  K and the King profile sphere. Since the size of the PGC at this stage is unknown, we examine three different cases for an initial radius of  $R_i = 150, 200, \text{ and } 300$  pc.

In all three cases, the initial density of the central region is high enough for efficient cooling to occur, so that the temperature of the central region decreases rapidly to  $\sim 10^2$  K. Due to the high density and low temperature ( $\sim 10^2$  K), a burst of star formation occurs in the central region in all cases. After the first star formation, the central region becomes the heating region and the temperature of the central region increases gradually.

At  $t \sim 6$  Myr, Type II supernovae start to occur and the temperature of the heating region increases rapidly to  $T \sim 10^6$  K. The left panel of Figure 5 shows the evolutionary changes in the central temperature for  $R_i = 150$  pc. Such a high temperature region expands and the central density begins to decrease (see the right panel of Figure 5). The expansion of the central region leads to the formation of a shell structure as seen in the evolution of the gas density profile (Figure 6). The density profile at  $t = 6$  Myr, clearly shows the shell structure. After that time, the shell expands outwardly (see the right panel of Figure 6).

The star formation after the shell formation occurs not in the central region but in the shell. Figure 7 show the change in the radius of the star forming region as a function of time for  $R_i = 150$  pc. We can see that the star forming region moves outward. At  $t = 10$  Myr, where we stop the computation for  $R_i = 150$  pc, the stellar mass reaches  $\sim 1.3 \times 10^5 M_\odot$ . This means that the star formation efficiency is  $\sim 13$  %. The bound stellar mass at  $t = 10$  Myr is  $\sim 10^5 M_\odot$  and the mass is comparable to the typical mass of globular clusters ( $\sim 10^5 M_\odot$ ). At  $t = 10$  Myr, the gas is almost removed from the central region. Figure 8 shows the projected particle positions of STAR particles (left panel) and the stellar density profile (right panel) at  $t = 10$  Myr. The STAR particle shows elongated shape (bar like shape). Such a shape is caused

by the radial orbit instability of the STARS formed at the large radius (Palmer & Papaloizou 1987). The central density of STARS is as high as  $\sim 100 M_\odot \text{ pc}^{-3}$  and the central velocity dispersion of the STARS is  $\sim 3 \text{ km s}^{-1}$ . This value of velocity dispersion is smaller than the observed value (Dubath, Meylan & Mayor 1997). We need to follow further evolution of the star clusters for proper comparison, which is not feasible with present code. The number of STAR particles at  $t = 10$  Myr is  $\sim 2500$ .

For  $R_i = 200$  pc and  $300$  pc, the overall evolution is similar to the case for  $R_i = 150$  pc and the stellar masses at  $t = 10$  Myr are  $\sim 8.5 \times 10^4 M_\odot$  and  $\sim 5.6 \times 10^4 M_\odot$ , respectively. The bound stellar mass are  $\sim 5 \times 10^4 M_\odot$  for both case. These results are summarized in Table 1. The initial concentration correlates with the final stellar mass and the final concentration of stellar system. In order for the stellar system as massive as  $10^5 M_\odot$  to form, the PGC should be as compact as  $R_i < 200$  pc ( $\rho_c > 10^{-22} \text{ g cm}^{-3}$ ) for the metal-free condition.

## 4.2. Evolution of the metal-rich PGC

The chemical composition of stars in globular clusters is one of the most crucial quantities to constrain the model for the globular cluster formation. The assumption that PGC initially has some heavy elements is quite reasonable. Actually, all globular clusters in our galaxy have some metals of  $[\text{Fe}/\text{H}] = -2.25 - 0$ . The metallicity distribution of the globular clusters shows bimodal distributions (Harris 1991). From this fact, we choose the initial metallicity of the cloud ranging from  $[\text{Fe}/\text{H}] = -2$  to  $0$ . For comparison, we will evolve the lower metallicity ( $[\text{Fe}/\text{H}] = -3$ ) cloud. The results presented in this section are obtained for case B.

Using the same initial conditions presented in section 4.1, we evolve the PGC for different metallicity. For the initial radius of the cloud, we set  $R_i = 300$  pc. The first star formation occurs in the central region and the STARS heat up the surrounding matter to gradually increase the temperature of the central region. At  $t \sim 6$  Myr, Type II supernovae begin to occur and the temperature of the heating region increases rapidly to  $T \sim 10^6$  K. Figure 9 shows the evolutionary changes in the central temperature (left panel) and gas density (right panel) for  $[\text{Fe}/\text{H}] = -2$ . The evolution for  $[\text{Fe}/\text{H}] = -2$  is very similar to the evolution of the metal-free cloud. After  $t \sim 6$  Myr, the central high density region makes the shell structure as in the metal-free case. At  $t = 10$  Myr, the bound stellar mass reaches  $\sim 1.0 \times 10^5 M_\odot$  for  $[\text{Fe}/\text{H}] = -2$ .

For higher metallicity, i.e.,  $[\text{Fe}/\text{H}] \geq -1$ , details of the evolution are somewhat different. We compare the central temperature evolution for different metallicity in Figure 10. Due to the different cooling rate, the initial decrease in the temperature is larger for higher metallicity. This difference leads to different star formation history as shown in Figure 11. For  $[\text{Fe}/\text{H}] = 0$ , the initial star burst is very intense and then the SFR decrease sharply becoming lower than the low metallicity case after  $t = 1$  Myr. This is because heating due to the stellar winds much larger for higher metallicity (see Section 2.3.1). The rise in the SFR after  $t = 6$  Myr for  $[\text{Fe}/\text{H}] = 0$  is caused by Type II supernovae.

The SFR for  $[\text{Fe}/\text{H}] = -1$  is almost constant during the evolution. For  $[\text{Fe}/\text{H}] = -2$ , the first star formation oc-

curs at  $t \sim 0.5$  Myr because of the lower cooling rates. The SFR after  $t = 2$  Myr is almost constant but lower than for  $[\text{Fe}/\text{H}] = -1$ .

The bound stellar mass at  $t = 10$  Myr is  $\sim 1.5 \times 10^5 M_\odot$  and  $1.0 \times 10^5 M_\odot$  for  $[\text{Fe}/\text{H}] = -1$  and 0, respectively. The reason for such a metallicity dependence is summarized below. The bound stellar mass, the central stellar density, and the central velocity dispersion are summarized in Table 1. The results depend on the metallicity as follows:

1. The initial metallicity significantly affects the star formation history. This difference makes the subsequent evolution different.
2. For the higher metallicity, the final stellar mass at  $t = 10$  Myr is larger because of the more efficient cooling rate.
3. The bound stellar mass is not an increasing function of the initial metallicity. This is because heating due to the stellar winds is larger for higher metallicity.
4. For lower metallicity ( $[\text{Fe}/\text{H}] = -3$ ), only  $\sim 3 \times 10^3 M_\odot$  stars form. This implies that  $[\text{Fe}/\text{H}] \geq -2$  is necessary to form globular clusters of  $\sim 10^5 M_\odot$  if  $R_i \sim 300$  pc.

#### 4.3. Parameter dependence

In this subsection, we describe the dependence of the results on various numerical parameters, e.g., the initial particle number ( $N_i$ ) and the feedback radius ( $R_f$ ). We use the metal-rich cloud of  $[\text{Fe}/\text{H}] = -1$  as a reference model, where  $N_i = 5000$  and  $R_f = 3$  pc.

First, we describe the dependence on the initial particle number. With larger (smaller) number of initial gas particles, the initial masses of the gas particles are smaller (larger). There is no strong dependence on the mass of the gas particles in our star formation recipes because Eq. (12) does not include the mass of the gas particles. However, the maximum density ( $\rho_{\text{max}}$ ) that can be represented in the SPH method depends on the mass of the gas particles, which may produce weak dependence on  $N_i$ . To confirm this, we evolve the model with  $N_i = 10^4$ . The overall evolution is almost indistinguishable to the reference model. The stellar mass at  $t = 10$  Myr becomes  $\sim 1.2 \times 10^5 M_\odot$ , which is slightly smaller than  $1.3 \times 10^5 M_\odot$  in the reference model. For  $N_i = 2500$  (a half of the reference model), we obtain the stellar mass of  $\sim 1.5 \times 10^5 M_\odot$ . In Figure 12, we compare the gas density profiles at  $t = 10$  Myr for different  $N_i$ . The position of the shell for the model with  $N_i = 10^4$  is different from other models because of the smaller stellar mass at the same epoch. However, all three models show the similar density profiles so that we conclude that the dependence on the initial gas particle number is weak. Thus,  $N_i \sim 5000$  is sufficient for the current numerical model.

Secondly, we describe the dependence on the size of the feedback radius  $R_f$ . In our model, the cooling and the star formation are suppressed for the gas particles in heating phase. We therefore expect that the size of  $R_f$  affects the star formation history. With larger  $R_f = 5$  pc, the star formation rates are smaller and the final stellar mass ( $\sim 0.9 \times 10^5 M_\odot$ ) is smaller than  $1.3 \times 10^5 M_\odot$  in

the reference model ( $R_f = 5$  pc). On the other hand, we obtain the stellar mass of  $\sim 1.9 \times 10^5 M_\odot$  with smaller  $R_f (= 2$  pc). Within the reasonable range of  $R_f$  around 3pc, the final stellar mass changes by a factor of 0.7 - 1.5.

#### 4.4. Summary of the numerical results

The results of our calculations are summarized as follows (see also Table 1) :

1. In all cases, the overall evolution is similar. Initially, the star burst occurs in the central region. The central star burst is halted by the heating due to Type II supernovae. The heating cause the expansion of the central region and forms a shell structure. The subsequent star formation occurs in the shell.
2. For the metal-free collapse case, the stellar mass at  $t = 10$  Myr correlates with initial concentrations. To obtain the star cluster as massive as globular clusters ( $\sim 10^5 M_\odot$ ), the initial concentration of the PGC must be large enough, i.e.,  $R_i < 200$  pc.
3. For the metal-rich collapse, the initial metallicity significantly affects the evolution. To obtain the star cluster as massive as globular clusters, the initial metallicity must be as larger as  $[\text{Fe}/\text{H}] \sim -2$ . If the initial metallicity is low ( $[\text{Fe}/\text{H}] < -2$ ), very few stars form.
4. This suggests that during the initial phase of the galaxy formation, i.e., when the ISM contains little heavy element, the formation efficiency of the globular cluster is low.
5. The results is not strongly affected by the initial number of gas particles.  $N_i \sim 5000$  is sufficient for the current numerical model. The dependence on the feedback radius is more evident.

## 5. DISCUSSION

### 5.1. Star formation in the shell

In all our numerical models, a shell-like gaseous structure is formed. The formation of the shell-like structure of gases has also been reported in the simulations of the formation of dwarf elliptical galaxies (Mori et al. 1997; Mori, Yoshii, & Nomoto 1999). They argued that the difference in the density structure between normal ellipticals (de Vaucouleurs law) and dwarf ellipticals (exponential law) can be explained by the formation of such a shell-like structure and the star formation in the shell. The most crucial difference between the normal elliptical and the dwarf is their mass, and the less massive galaxy is more strongly affected by the energy inputs from stars. Similar argument may be applicable to our numerical models. In the case of the globular cluster formation, however, the mass is even smaller than the dwarf galaxies. Owing to this fact, the effect of the energy inputs from stars is more drastic so that the star formation in the shell is much less efficient than in the dwarf galaxies. Also, the stars formed in the shell is not gravitationally bound due to the outward velocity of the shell. Thus, the bound globular cluster consists of the stars formed before the shell formation. The stellar density of such stars is not affected by the shell formation and the star formation in the shell.

The chemical composition of stars in globular clusters is one of the most crucial quantities to constrain the model for the globular cluster formation. The stars in a globular cluster have almost the same heavy elements abundances (Suntzeff 1993). This small dispersion in metallicity ( $\sigma[\text{Fe}/\text{H}]$ ) suggests that the formation period of globular clusters is so short that the stars in globular clusters can be regarded to form almost simultaneously as shown in our numerical models.

Brown, Burkert & Truran (1991, 1995) suggested that the second generation stars would form in the shell and the self-enrichment could occur there. In our model, the star formation takes place in the shell after  $t = 5$  Myr (see Figure 7). However, when the stars form in the shell, the shell has not been enriched with newly ejected heavy metal as shown in the solid line in Figure 7. This line shows the radius of the metal-enriched region defined as  $r = (\Sigma r_i m_i) / (\Sigma m_i)$  by summing over the metal-enriched gas particles. The metal-enriched region expands outwardly but does not reach the star forming region, which implies that the self-enrichment does not occur in our model (we note that the star formation is suppressed in the gas particles near the STARS in our numerical model as described in section 2.3.3). In the present model, no external medium outside the cloud is included, because of technical difficulties in the SPH method (see, however, Nagasawa & Miyama (1987) for a possible improvement). If there exists external medium outside the cloud, the density of the shell would be higher and the star formation history would be different; this possibility needs further study to confirm.

### 5.2. Failed Globular clusters

When a PGC is an initially metal-free cloud or the initial metallicity of a PGC is low, the resulted mass and the central stellar density are lower than the observed mass and density of the globular clusters. Such “failed” globular clusters might be the field halo stars. Another possibility is a open cluster. Typical age of open clusters in our galaxy is  $\tau < 10^9$  yr. However, there also exist such old open clusters as  $\tau > 10$  Gyr (Friel 1995). The age of the most old open cluster is comparable to the age of globular clusters. The central density of the “failed” globular cluster is as low as the central density of typical open clusters. Thus, the formation processes of such old open clusters may be the similar to our model of globular cluster formation but starting from lower initial concentration. Very old open clusters might be the debris of “failed” globular clusters and there might have existed many more open clusters at the formation of our galaxy.

## 6. CONCLUSIONS

For the processes of globular clusters formation, only the qualitative scenarios have been discussed previously (Fall & Rees 1985; Lin & Murray 1996). In this paper, we present the first attempt to simulate the globular cluster formation with three-dimensional hydrodynamical method, which includes the star formation and its feedback effects. We assume that, in the collapsing galaxy, isothermal cold clouds form through thermal condensations and become proto-globular clouds. We obtain the size of proto-globular clouds by means of the linear stability analysis (Figure 3) and compute the evolution of the

inner region of the PGC starting from various initial radius  $R_i$ . The results of our calculations are summarized as follows:

1. In order for the globular cluster-like system to form from a metal-free PGC, the initial concentration of the PGC must be large enough.
2. It is required that the metallicity of a PGC is high enough to produce the globular cluster-like system. In our calculations, the required metallicity is estimated to be  $[\text{Fe}/\text{H}] \geq -2$ .
3. In all cases, the shell like structure of the gas forms. Although the star formation occurs in the shell, the self-enrichment is not seen to occur.

Based on the earlier qualitative works and the present quantitative results, the processes of globular clusters formation in the proto-galaxy can be understood as follows:

1. In the collapsing proto-galaxy, the first generation stars of  $M \sim 10^2 M_\odot$  form due to the efficient cooling by hydrogen molecules. Such population III stars eject the gas with heavy elements and chemically contaminate the proto-galaxy gases.
2. Such first generation stars radiate dissociative photons, and the entire proto-galaxy is settled down to ionization equilibrium.
3. With equilibrium cooling, the density perturbation grows due to thermal instability, and forms an isothermal cloud with a density structure of  $\propto r^{-2}$ . Such clouds are the proto-cloud of globular clusters.
4. When the density of the PGC becomes high enough, the burst of star formation occurs. Some high density clouds produce the globular clusters, and others may produce the field stars and/or the halo open clusters.
5. During the formation of the galaxy, the formation efficiency of the globular cluster become significantly large when the metallicity of the PGC become as large as  $[\text{Fe}/\text{H}] \sim -2$ .

As mentioned in section 5.1, we do not take account of the effect of the external medium in the present calculations. If we include the effect of the external medium, the structure of the shell may be different and further star formation may occur in that shell. Brown, Burkert & Truran (1995) suggested that only a few supernovae per Myr is sufficient to reverse the contraction of the  $10^6 M_\odot$  cloud. Such an effect of the external medium needs to be studied.

The globular cluster formation is considered to occur not only in the proto-galaxies but also in the present galaxies, e.g., LMC, SMC, and interacting galaxy NGC4038/NGC4039. In such environment, different formation processes would take place, which correspond to the tertiary models (Kumai, Basu, & Fujimoto 1993). In the case of NGC4038/NGC4039 (the Antennae galaxies), many globular clusters are being produced by galaxy merging. Detail formation processes of globular clusters in such systems needs to be studied. Also, the effect of the



formation of many globular clusters on the galaxy merging process needs a further study.

We would like to thank the anonymous referee for the valuable suggestions to improve the manuscript. Also, we would like to thank G. Mathews, J. Truran, T. Shigeyama

and S. Zwart for useful discussion and comments. This work has been supported by JSPS Research Fellowships for Young Scientists (7664), and in part by the grant-in-Aid for COE Scientific Research (07CE2002) of Ministry of Education, Science, Culture, and Sports of Japan.

#### REFERENCES

- Abbot, D.C., 1982, *ApJ*, 263, 723  
 Brown, J.H., Burkert, A., & Truran, J.W., 1991, *ApJ*, 376, 115  
 Brown, J.H., Burkert, A., & Truran, J.W., 1995, *ApJ*, 440, 666  
 David, L.P., Forman, W., & Jones, C., 1990, *ApJ*, 459, 29  
 Dubath, P., Meylan, G., & Mayor, M., *A&A*, 324, 505  
 Ebert, R., 1955, *Zs. Ap.*, 37, 217  
 Elmergreen, B.G., Efremov, Y., Pudritz, R.E., & Zinnecker, H., 1999, *astro-ph/9903136*  
 Fall, S.M., & Rees, M.J., 1985, *ApJ*, 298, 18  
 Fall, S.M., & Rees, M.J., 1987, in *IAU Symposium 126, Globular cluster systems in galaxies*, eds. Grindlay, J. & Philip, D. (Dordrecht: Kluwer), 323  
 Field, G.B., 1965, *ApJ*, 142, 531  
 Friel, E.D., 1995, *Annu. Rev. Aston. Astrophys.*, 33, 381  
 Friedli, D., & Benz, W., 1995, *A&A*, 301, 649  
 Gingold, A., & Monaghan, J., 1977, *MNRAS*, 181, 37  
 Harris, W.E., 1991, *Annu. Rev. Aston. Astrophys.*, 29, 543  
 Ho, L.C., & Filippenko, A.V., 1996, *ApJL*, 466, 83  
 Katz, N., 1992, *ApJ*, 391, 502  
 Katz, N., Weinberg, D.H., & Hernquist, L., 1996, *ApJS*, 105, 19  
 Kumai, Y., Basu, B., & Fujimoto, M., 1993, *ApJ*, 404, 144  
 Leitherer, C., Robert, C., & Drissen, L., 1992, *ApJ* 401, 596  
 Lin, D.N.C., & Murray, S.D., 1996, in *IAU Symposium 174, Dynamical evolution of star clusters*, eds. Hut., P. & Makino, J. (Dordrecht: Kluwer), 283  
 Lucy, L., 1977, *AJ*, 82, 1013  
 McCrea, W.H., 1957, *MNRAS*, 117, 562  
 Meerson, B., 1996, *Reviews of Modern Physics*, 68, 1, 215  
 Meylan, G., Heggie, D.C., 1997, *A&AR*, 8, 1  
 Mori, M., Nakasato, N., Yoshii, Y., & Nomoto, K., 2000, in *preparation*  
 Mori, M., Yoshii, Y., Tsujimoto, T., & Nomoto, K., 1997, *ApJL*, 478, 21  
 Mori, M., Yoshii, Y., & Nomoto, K., 1999, *ApJ*, 511, 585  
 Murray, S.D., & Lin, D.N.C., 1993, in *ASP Conf. Ser. Vol. 48, The Globular Cluster-Galaxy Connection*, eds. Smith, G.H., & Brodie, J.P. (San Francisco: Astronomical Society of the Pacific), 738  
 Nagasawa, M., & Miyama, S.M., 1987, *Prog. Theor. Phys.*, 78, 1250  
 Nakasato, N., Mori, Tsujimoto, T., Mathews, G., & Nomoto, K., 1996, in *IAU Symposium 174, Dynamical Evolution of Star Clusters*, eds. Hut, P., & Makino, J. (Dordrecht: Kluwer), 397  
 Nakasato, N., Mori, M., & Nomoto, K., 1997, *ApJ*, 484, 608  
 Nakasato, N., Mori, & Nomoto, K., 1999, in *IAU Symposium 187, Cosmic Chemical Evolution*, eds. Truran, J.W., & Nomoto, K. (Dordrecht: Kluwer), in press  
 Navarro, J.F., & White, S.D.M., 1993, *MNRAS*, 265, 271  
 Nomoto, K., Hashimoto, M., Tsujimoto, T., Thielemann, F.-K., Kishimoto, N., Kubo, Y., & Nakasato, N., 1997, *Nucl. Phys. A.*, 616, 79c  
 Osterbrock, D.E., 1974, *Astrophysics of Gaseous Nebulae* (San Francisco: W. H. Freeman and Company)  
 Palmer, P.L., & Papaloizou, J., 1987, *MNRAS*, 224, 1043  
 Parker, E.N., 1953, *ApJ*, 117, 431  
 Peebles, P.J.E., & Dicke, R.H., 1968, *ApJ*, 154, 891  
 Schmidt, M., 1959, *ApJ*, 129, 243  
 Shapiro, P.R., & Kang, H., 1987, *ApJ*, 318, 32  
 Spitzer, L., Jr., 1978, *Physical Processes in the Interstellar Medium* (New York: Wiley Interscience)  
 Steinmetz, M., & Müller, E., 1994, *A&A*, 281, 97  
 Sugimoto, D., Chikada, Y., Makino, J., et al., 1990, *Nature*, 345, 33  
 Suntzeff, N., 1993, in *ASP Conf. Ser. Vol. 48, The Globular Cluster-Galaxy Connection*, eds. Smith, G.H., & Brodie, J.P., (San Francisco: Astronomical Society of the Pacific), 167  
 Sutherland, R.S., & Dopita, M.A., 1993, *ApJS*, 88, 253  
 Thacker, R.J., Tittley, E.R., Pearce, F.R., Couchman, H.M.P., & Thomas, P.A., 1998, *astro-ph/989221*  
 Tsujimoto, T., Nomoto, K., Yoshii, Y., Hashimoto, M., Yanagida, S., & Thielemann, F.-K., 1996, *MNRAS*, 277, 945

TABLE 1  
THE SUMMARY OF THE NUMERICAL RESULTS

$R_i^a$	[Fe/H] <sup>b</sup>	Mass <sup>c</sup>	$\rho_c^d$	$\sigma_c^e$
150 pc	no metal	$1.0 \times 10^5 M_\odot$	$10^{2.5} M_\odot \text{ pc}^{-3}$	$2.98 \text{ km s}^{-1}$
200 pc	no metal	$5.1 \times 10^4 M_\odot$	$10^{1.1} M_\odot \text{ pc}^{-3}$	$1.87 \text{ km s}^{-1}$
300 pc	no metal	$5.5 \times 10^4 M_\odot$	$10^{1.4} M_\odot \text{ pc}^{-3}$	$3.66 \text{ km s}^{-1}$
300 pc	0	$1.0 \times 10^5 M_\odot$	$10^{2.0} M_\odot \text{ pc}^{-3}$	$3.21 \text{ km s}^{-1}$
300 pc	-1	$1.5 \times 10^5 M_\odot$	$10^{2.0} M_\odot \text{ pc}^{-3}$	$2.33 \text{ km s}^{-1}$
300 pc	-2	$1.0 \times 10^5 M_\odot$	$10^{1.7} M_\odot \text{ pc}^{-3}$	$2.68 \text{ km s}^{-1}$
300 pc <sup>f</sup>	-3	$2.9 \times 10^3 M_\odot$		

NOTE.— <sup>a</sup>The initial radius of the PGC.  
<sup>b</sup>The initial metallicity ([Fe/H]) of the PGC.  
<sup>c</sup>The bound stellar mass at  $t = 10$  Myr.  
<sup>d</sup>The central stellar density at  $t = 10$  Myr.  
<sup>e</sup>The central stellar velocity dispersion at  $t = 10$  Myr.  
<sup>f</sup>  $\rho_c$  and  $\sigma_c$  is omitted of this case.

TABLE 2  
THE DEPENDENCE ON NUMERICAL PARAMETERS

$N_i^a$	$R_f^b$	Mass <sup>c</sup>
5000	3 pc	$1.5 \times 10^5 M_\odot$
2500	3 pc	$1.5 \times 10^5 M_\odot$
$10^4$	3 pc	$1.2 \times 10^5 M_\odot$
5000	2 pc	$1.9 \times 10^5 M_\odot$
5000	5 pc	$8.6 \times 10^4 M_\odot$

NOTE.— <sup>a</sup>Used initial gas particle number.  
<sup>b</sup>The feedback radius.  
<sup>c</sup>The stellar mass at  $t = 10$  Myr.

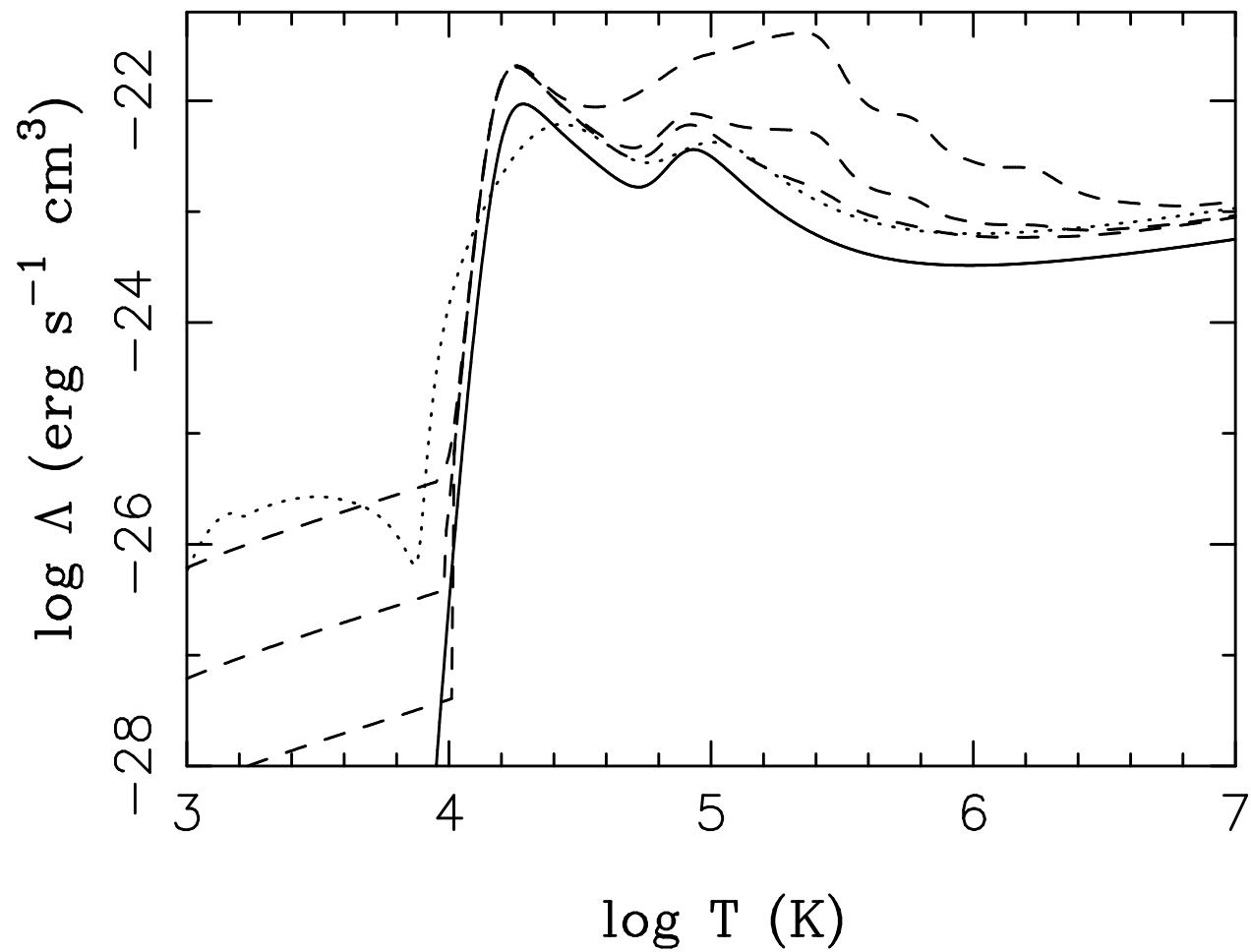


FIG. 1.— The various cooling rates used in SPH code. The solid and dotted show the cooling rates for cases A and C, respectively. The dashed lines show the cooling rates for case B. From the top to the bottom line, each line corresponds to  $[\text{Fe}/\text{H}] = -1, -2$  and  $-3$ , respectively.

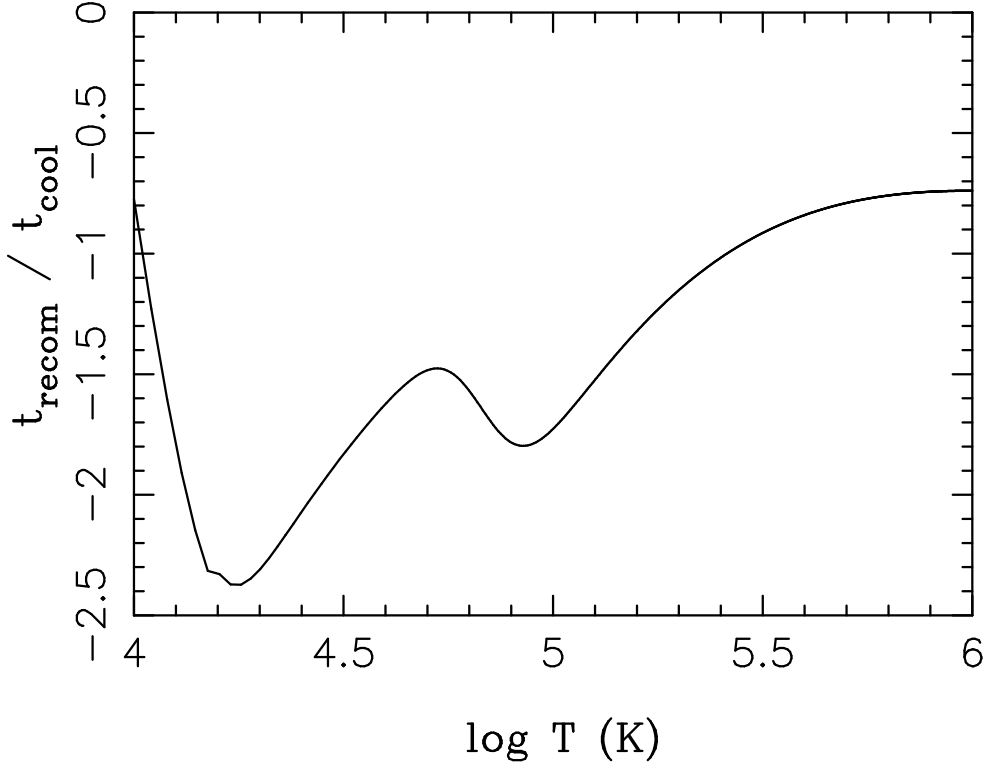


FIG. 2.— The ratio between the recombination time of hydrogen and the cooling time ( $t_{\text{recom}}/t_{\text{cool}}$ ) as a function of the temperature.

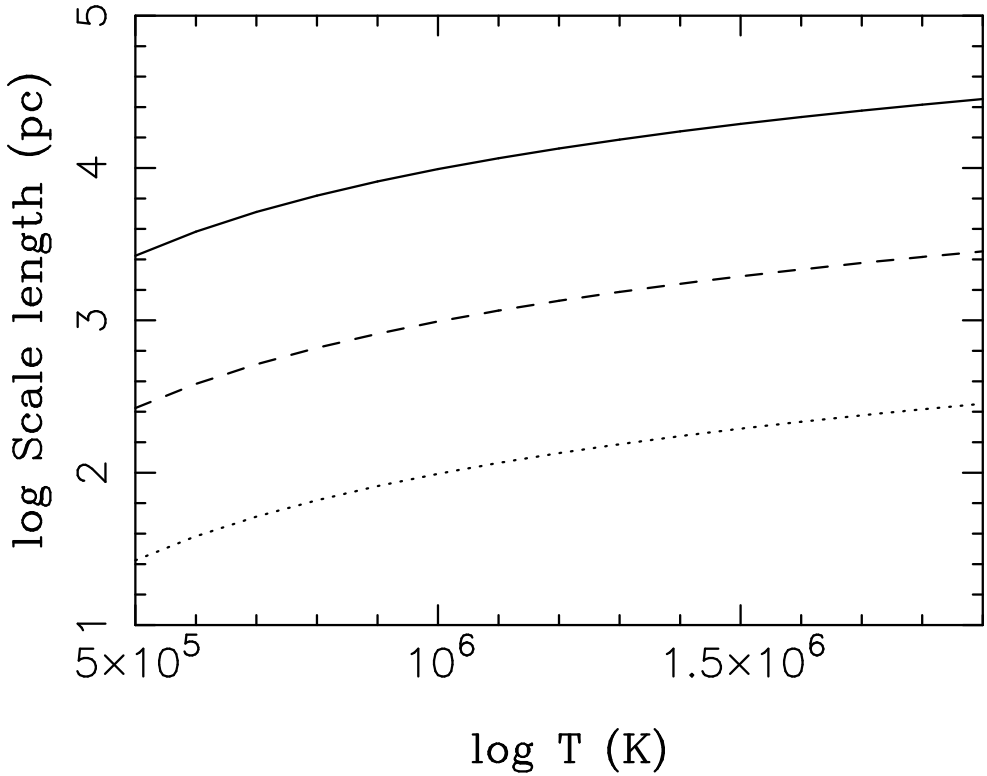


FIG. 3.— The estimated scale length of a proto-globular cloud corresponding to the maximum growth rate in Eq. (22). The solid, dashed, and dotted lines correspond to  $\rho_0 = 1.0 \times 10^{-25}$ ,  $1.0 \times 10^{-24}$ , and  $1.0 \times 10^{-23}$  g cm $^{-3}$ , respectively.

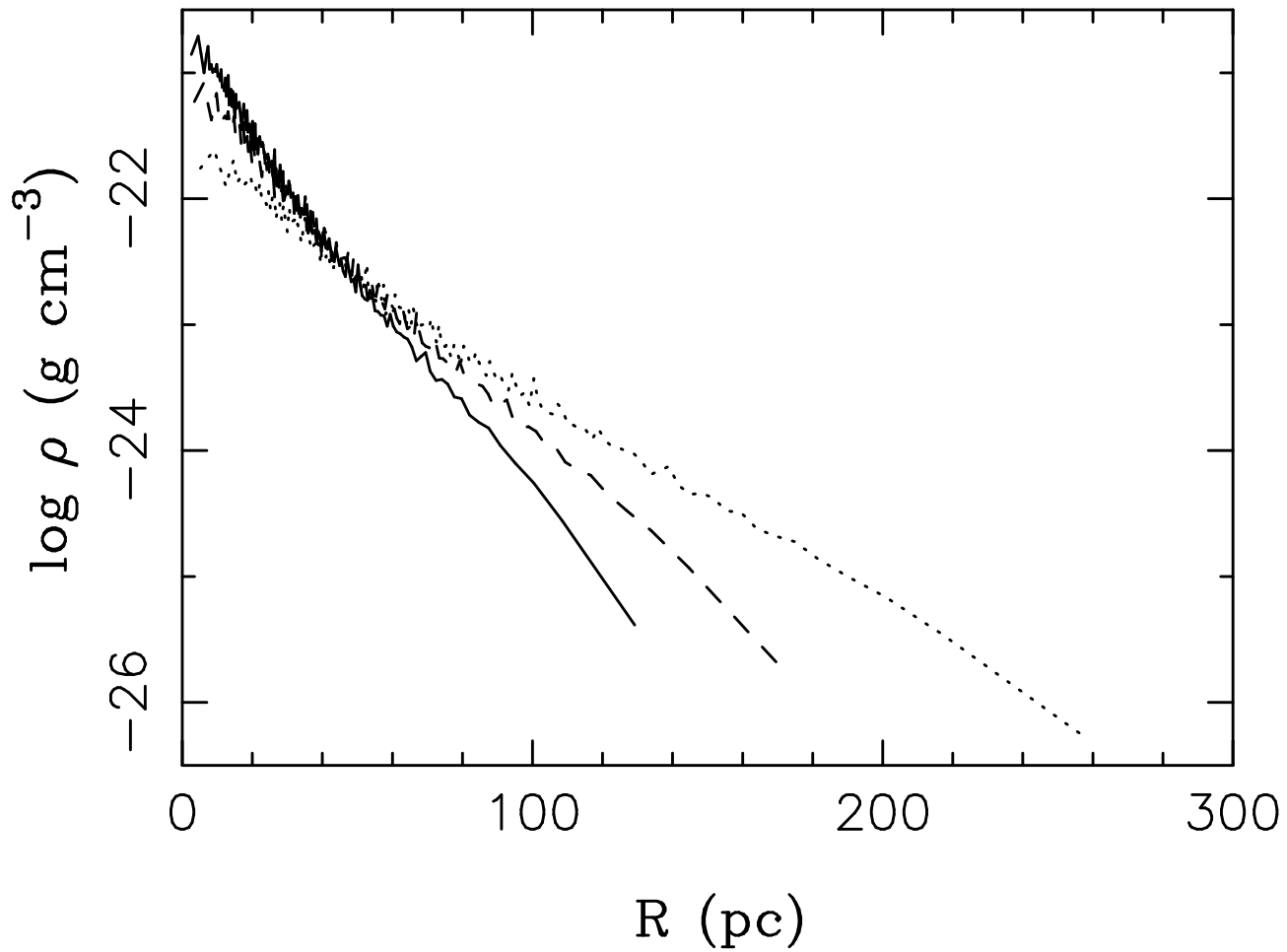


FIG. 4.— The initial gas density ( $\text{g cm}^{-3}$ ) profile for the King profile case. The solid, dashed, and dotted lines show the profiles for  $R_i = 150, 200,$  and  $300$  pc, respectively.

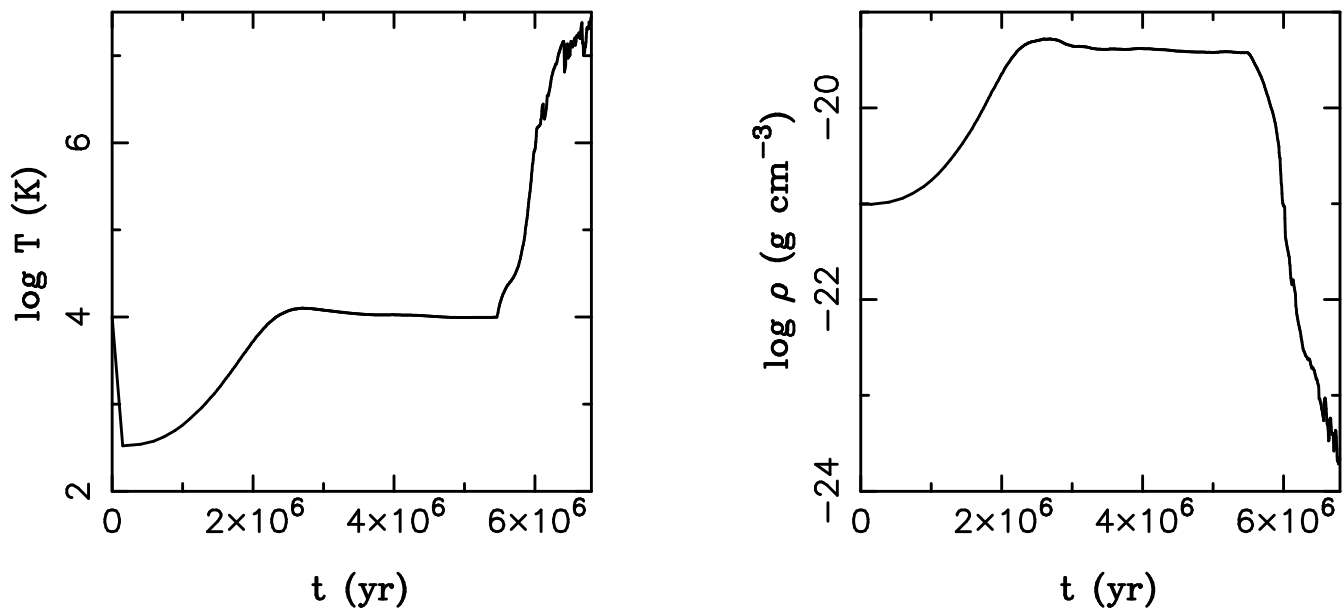


FIG. 5.— The evolutionary changes in the central temperature (left panel) and gas density (right panel) are shown for the metal-free collapse with  $R_i = 150$  pc.

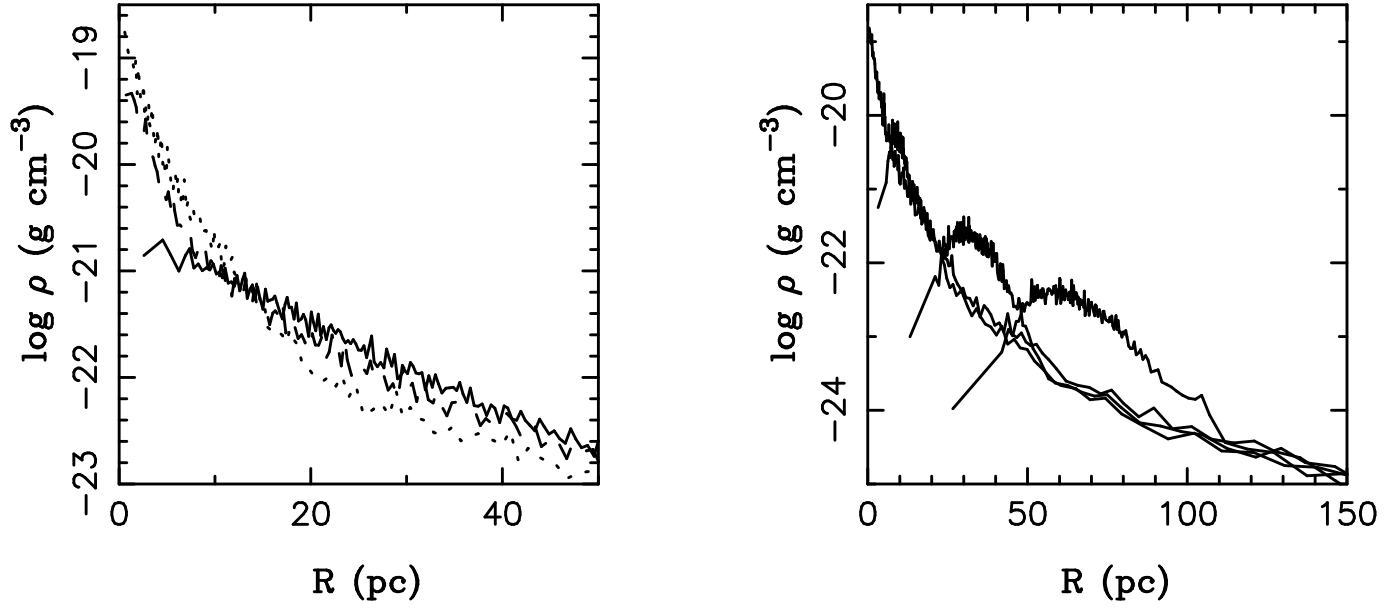


FIG. 6.— The gas density profile as a function of radius (pc). left: The solid, dashed and dotted lines respectively shows the profile at  $t = 0, 2, 4$  Myr. right: The solid lines with the decreasing central density correspond to  $t = 5, 6, 7, 8$  Myr.

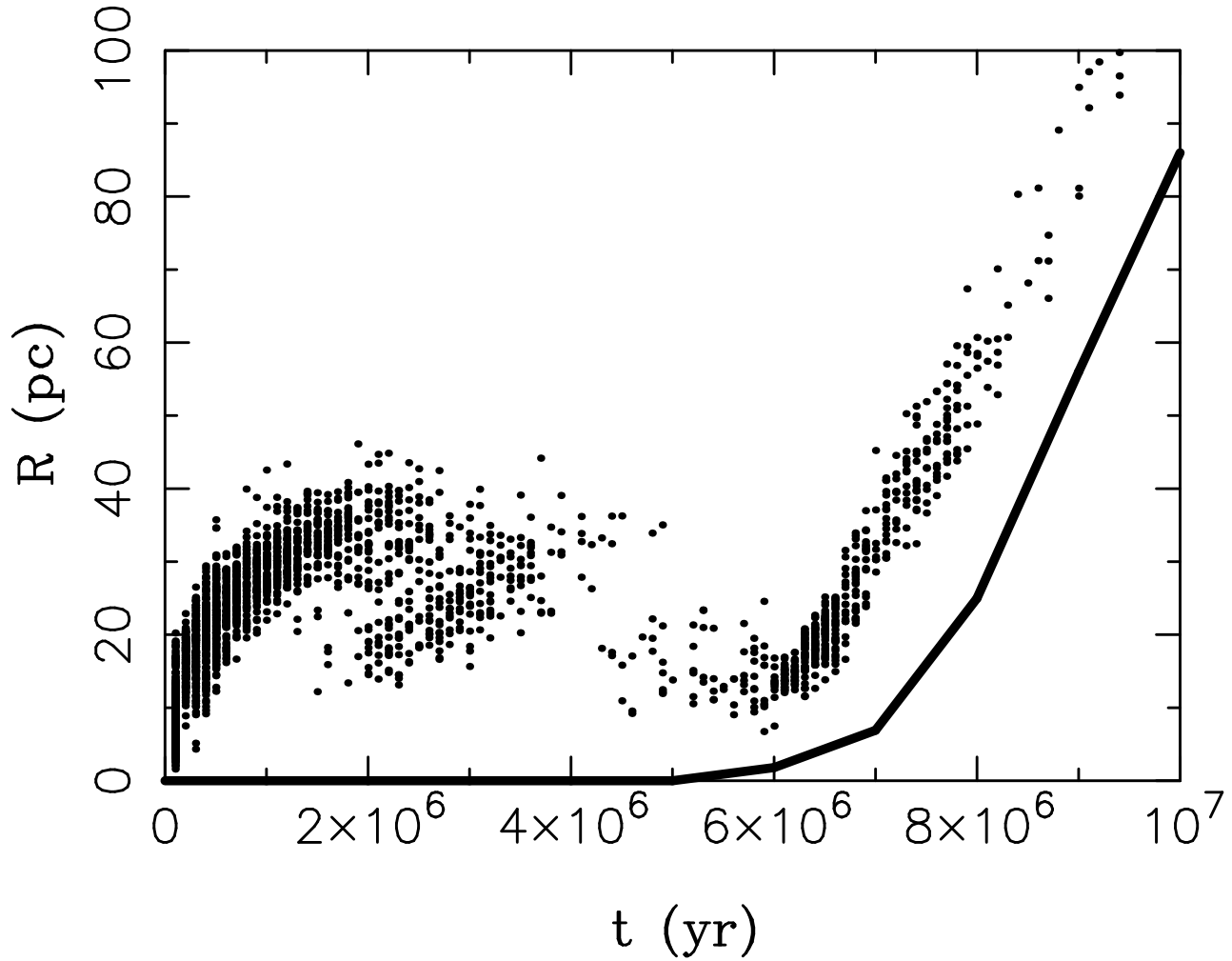


FIG. 7.— The radius (pc), at which stars form, as a function of time (yr) for the metal-free collapse with  $R_i = 150$  pc.

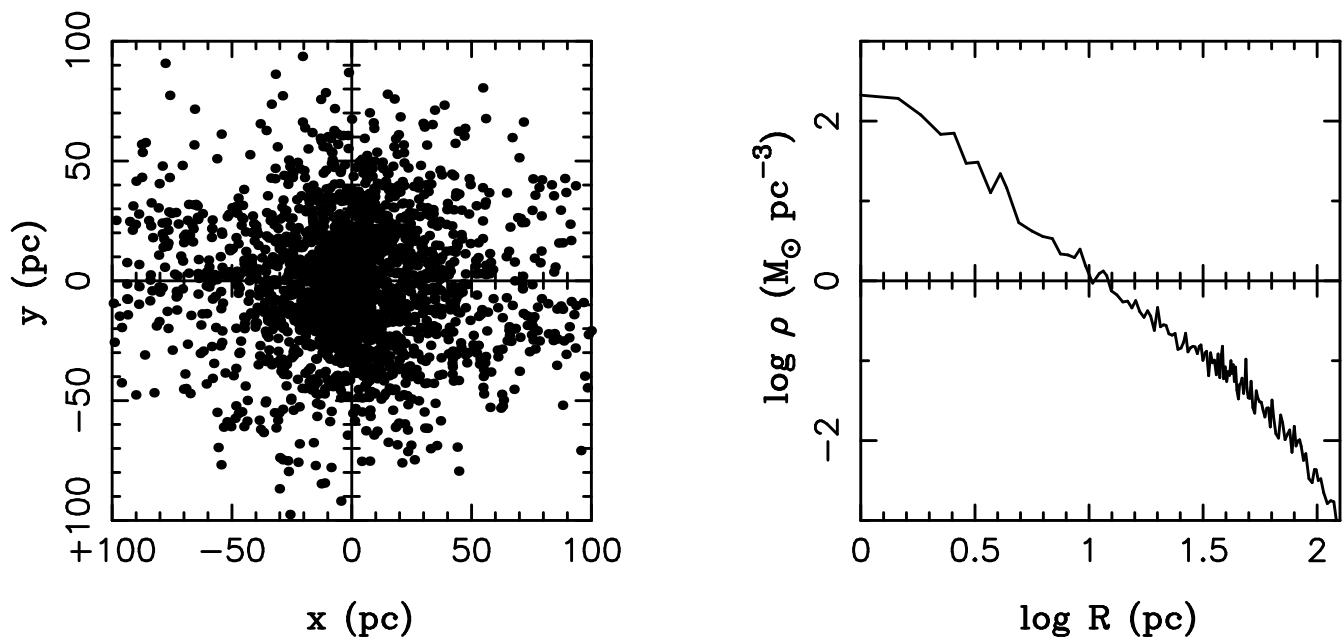


FIG. 8.— The projected position of particles at  $t = 10$  Myr for metal-free collapse with  $R_i = 150$  pc (left panel). The stellar density profile at  $t = 10$  Myr for the same model.

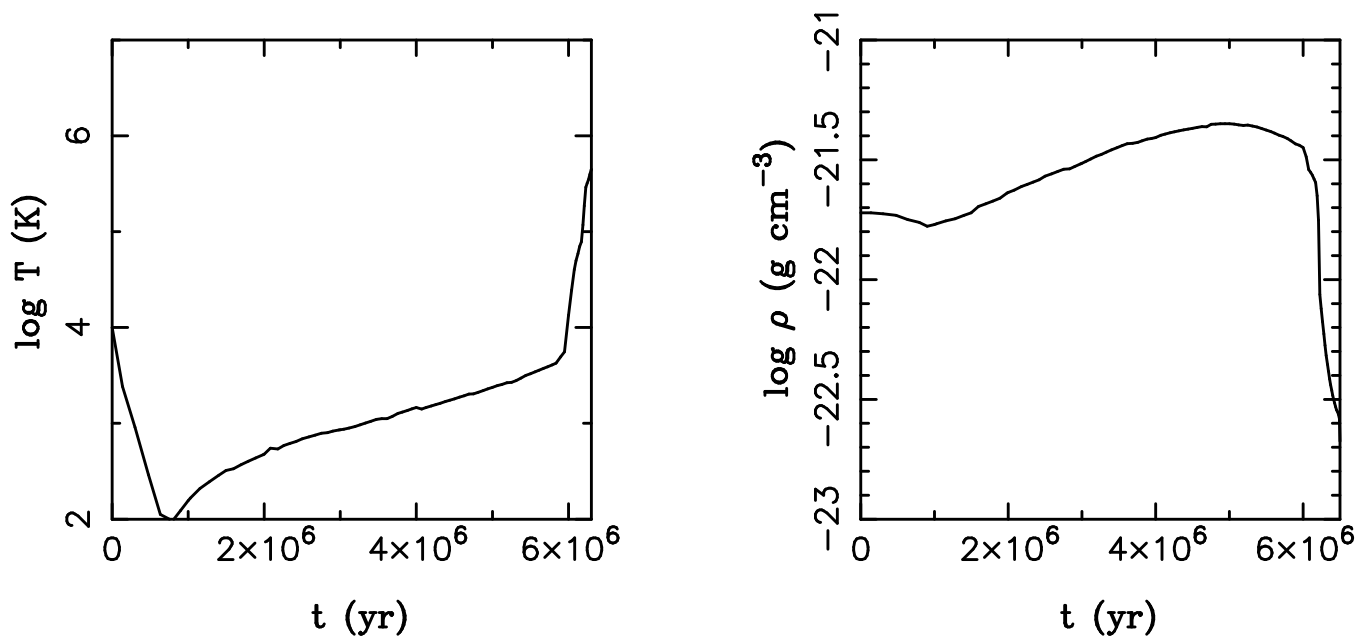


FIG. 9.— The evolutionary changes in the central temperature (left panel) and gas density (right panel) are shown for the collapse of  $[\text{Fe}/\text{H}] = -2$  sphere.

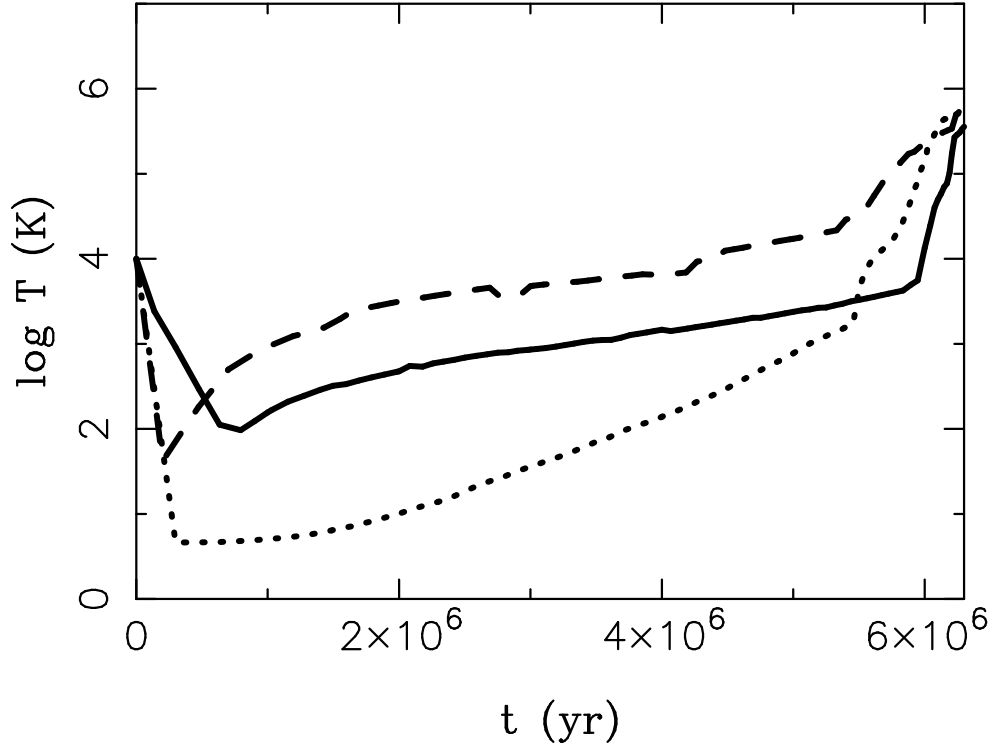


FIG. 10.— The evolutionary changes in the central temperature for the collapse of  $[\text{Fe}/\text{H}] = -2$  (solid line),  $-1$  (dashed line) and  $0$  (dotted line) sphere.

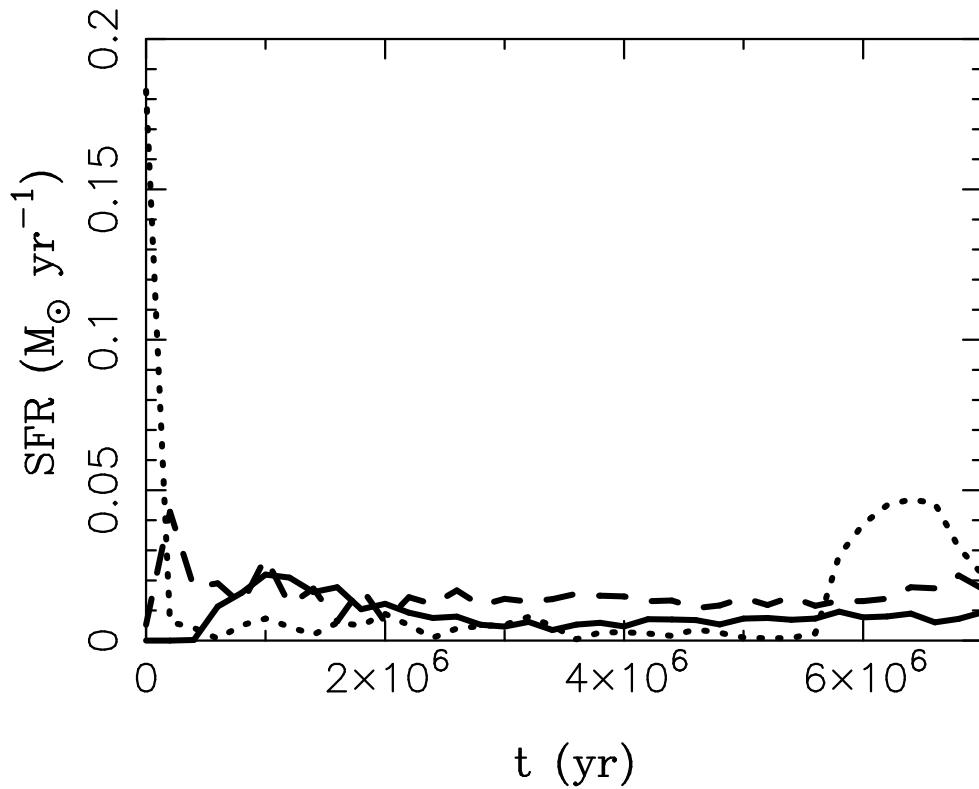


FIG. 11.— The comparison of SFR as a function of time for  $[\text{Fe}/\text{H}] = -2$  (solid line),  $-1$  (dashed line) and  $0$  (dotted line).



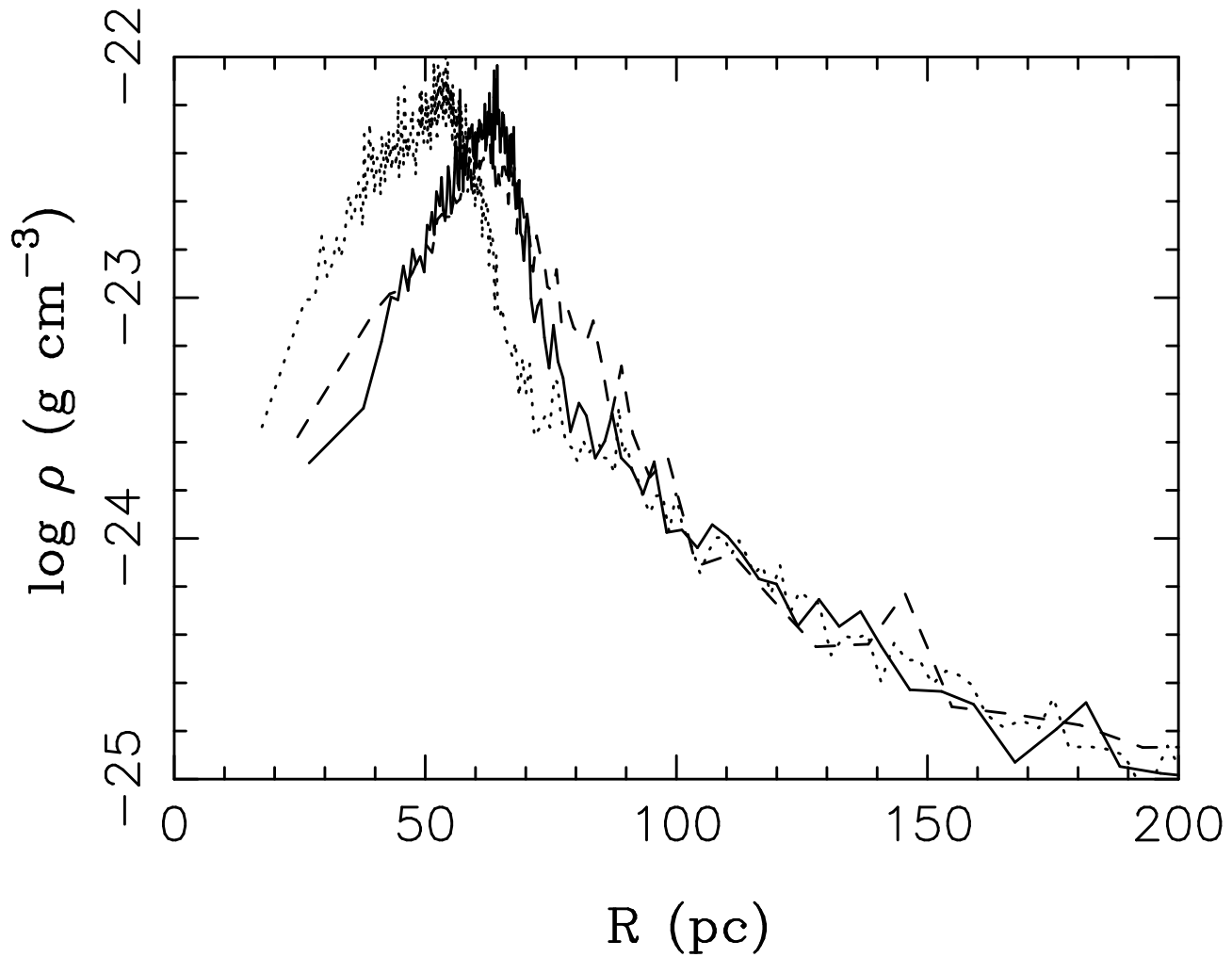


FIG. 12.— The comparison between the reference model (solid line) and other model. The dashed line corresponds to the model with  $N_i \sim 2500$ . The dotted line corresponds to the model with  $N_i \sim 10000$ .